Supporting information

Twist-angle-dependent momentum-space direct and indirect interlayer excitons in WSe_2/WS_2 heterostructure†

Jiajun Chen,†[a] Xiaofei Yue,†[a] Yabing Shan,[a] Huishan Wang,[b] Jinkun Han,[a] Haomin Wang,[b] Chenxu Sheng,[a] Laigui Hu,[a] Ran Liu,[a] Weihuang Yang,*[c] Zhi-Jun Qiu*[a] and Chunxiao Cong*[ad]

[a] *State Key Laboratory of ASIC & System, School of Information Science and Technology, Fudan University, Shanghai 200433, China.*

[b] *State Key Laboratory of Functional Materials for Informatics, Shanghai Institute of Microsystem and Information Technology, Chinese Academy of Sciences, Changning Road 865, Shanghai 200050, China.*

[c] *Engineering Research Center of Smart Microsensors and Microsystems, Ministry of Education, College of Electronics and Information, Hangzhou Dianzi University, Hangzhou 310018, China.*

[d] *Yiwu Research Institute of Fudan University, Chengbei Road, Yiwu City, 322000 Zhejiang, China.*

† These authors contributed equally to this work

† Electronic Supplementary Information (ESI) available. See DOI:

Fig. S1 (a) and (b) show the optical image and the fluorescence (FL) image of the WSe_2/WS_2 heterostructures. the FL image shows the strong quench in the heterostructure area, which indicates good contact and strong charge transfer between two layers. **Fig. S1** (c) shows the typical Raman spectrum of the WSe_2/WS_2 heterostructures, the peak located at ~248 cm^{-1}, ~258 cm^{-1} and ~416 cm^{-1} corresponding to the in-plane vibration mode and out-of-plane vibration mode of WSe_2 ($E_{2g}{}^1(WSe_2)$, $A_{1g}(WSe_2)$) and out-of-plane vibration mode of WS_2 ($A_{1g}(WS_2)$), the peak located at ~350 cm^{-1} can be fitted into three peaks, with the peaks at ~347 cm^{-1}, ~340 cm^{-1} and ~353 cm^{-1} are corresponding to the longitudinal acoustic mode 2LA(*M*) and the vibration mode E'(*M*) and E'(*Γ*). The frequency difference between A_{1g} and E_{2g} are ~10 cm^{-1} (WSe_2) and ~63 cm^{-1} (WS_2), which confirm the nature of the monolayer material. **Fig. S1** (d) shows the typical PL spectra of WSe_2 and WS_2, the peaks located at ~1.67eV and ~1.93eV corresponding to the intralayer excitons of WSe_2 and WS_2, these results also confirm the high quality of our sample. **Fig. S1** (e) shows the Raman spectra of the WSe_2/WS_2 heterostructure with different twist angles.

In order to determine the twist angle between two layers, the polarization-resolved second-harmonic-generation (SHG) microscopy was performed. **Fig. S2** (a) shows the polar plots of the SHG intensity of monolayer WSe_2 and five WSe_2/WS_2 heterostructures with specific twist angles. For parallel polarization SHG measurement, the SHG intensity is maximum if the polarization axis of the light is along an armchair direction, and the SHG intensity yielding an $I_{SHG} \propto \cos^2(3\theta-\theta_0)$, where θ_0 is the angle between the armchair direction and the polarization axis of the light. Combined with the intensity mapping measurements of the total SHG intensity (as shown in figure S2 (b)), the twist angle between two layers can be well-determined.[1] Figure S2 (c) shows the measured ratio of the SHG intensity from the heterostructure to the monolayer as a function of twist angles θ. Ideally, the SHG intensity of heterostructure with perfectly aligned ($\theta=0^o$) $I_{Heterostructure}$ is expected to be four times that of the SHG intensity of monolayer I_{WSe_2}.[2, 3] However, the SHG signal of aligned heterostructure is only ~2 times that of the monolayer, which may result from the absorption of electromagnetic waves in materials and the underlying substrate.[2]

Fig. S3 (a) shows the PL spectrum of the WSe_2/WS_2 heterostructure. (b) and (c) are the PL intensity mapping at ~1.4 eV of the WSe_2/WS_2 heterostructure with a twist angle of 59.1^o

and 2.1°, respectively. It shows this peak exists only in the heterostructure region which also confirms the nature of the interlayer exciton not the defect-trapped state.[4] Meanwhile, the uniform distribution of the interlayer exciton indicates good conduct between the two layers.

Fig. S4 shows the polarization-resolved SHG measurements of the WSe_2/WS_2 fabricated by CVD-grown samples. The results show that the twist angle between the two layers is 1.8°.

In order to eliminate the possibility of the extraction and injection of electrons from the heterostructure by the electrode, we use hBN to shield the influence of the electrode in another heterostructure as shown in **Fig. S5**. The interlayer exciton shows the same trend with the change of voltage, which further confirms that the enhancement of interlayer exciton is a result from the interaction with interlayer exciton and the external electric field.

To further understand the mechanism behind these phenomena, we use DFT calculation to show the interlayer coupling between the two layers. **Fig. S6** shows the structures of WSe_2/WS_2 heterostructures with twist angles of 0°, 27.8°, 38.2° and 60°, respectively. The structure parameters after relaxation are shown in **table S1**. We noticed that the interlayer distance of WSe_2/WS_2 heterostructures with twist angles of 0° and 60° are smaller than the twist angle near 30°. This result is consistent with other reports, [5, 6] which proved the stronger interlayer coupling in the WSe_2/WS_2 heterostructures with twist angles of 0° and 60°. Meanwhile, the interlayer distance of WSe_2/WS_2 heterostructures with twist angles of 0° and 60° shows a slight difference, which is consistent with our experimental phenomenon that the interlayer exciton in WSe_2/WS_2 heterostructures with twist angles near 0° and 60° are different (as shown in figure 2). To further reveal the difference of interlayer coupling between WSe_2/WS_2 heterostructures with different twist angles, the differential charge densities $\Delta\rho(r)$ are calculated (as shown in **fig. S7**), which are defined as:

$$\Delta\rho(r) = \rho(r) - \rho_{WS_2}(r - r_i) - \rho_{WSe_2}(r - r_i)$$

where $\rho(r)$ is the charge density of the WSe_2/WS_2 heterostructure, $\rho_{WS_2}(r - r_i)$ and $\rho_{WSe_2}(r - r_i)$ are the charge density of monolayer WS_2 and WSe_2 respectively. The total charge transfer is shown in **Fig. S8**. The charge transfer is strongly enhanced when the twist angle of WSe_2/WS_2 heterostructures are near 0° and 60°, which are consistent with our experimental results.

Table S2 summarizes some other reports of interlayer exciton. Our work provides a simpler and more efficient method for regulating momentum-space direct and indirect excitons.

References

1. Van Der Zande, A. M.; Huang, P. Y.; Chenet, D. A.; Berkelbach, T. C.; You, Y.; Lee, G.-H.; Heinz, T. F.; Reichman, D. R.; Muller, D. A.; Hone, J. C., Grains and grain boundaries in highly crystalline monolayer molybdenum disulphide. *Nat. Mater.* **2013,** *12* (6), 554-561.
2. Hsu, W.-T.; Zhao, Z.-A.; Li, L.-J.; Chen, C.-H.; Chiu, M.-H.; Chang, P.-S.; Chou, Y.-C.; Chang, W.-H., Second harmonic generation from artificially stacked transition metal dichalcogenide twisted bilayers. *ACS Nano* **2014,** *8* (3), 2951-2958.
3. Van Der Zande, A. M.; Kunstmann, J.; Chernikov, A.; Chenet, D. A.; You, Y.; Zhang, X.; Huang, P. Y.; Berkelbach, T. C.; Wang, L.; Zhang, F., Tailoring the electronic structure in bilayer molybdenum disulfide via interlayer twist. *Nano Lett.* **2014,** *14* (7), 3869-3875.
4. Kremser, M.; Brotons-Gisbert, M.; Knörzer, J.; Gückelhorn, J.; Meyer, M.; Barbone, M.; Stier, A. V.; Gerardot, B. D.; Müller, K.; Finley, J. J., Discrete interactions between a few interlayer excitons trapped at a $MoSe_2$–WSe_2 heterointerface. *npj 2D Materials and Applications* **2020,** *4* (1), 1-6.
5. Huang, S.; Ling, X.; Liang, L.; Kong, J.; Terrones, H.; Meunier, V.; Dresselhaus, M. S., Probing the interlayer coupling of twisted bilayer MoS_2 using photoluminescence spectroscopy. *Nano Lett.* **2014,** *14* (10), 5500-5508.
6. Nayak, P. K.; Horbatenko, Y.; Ahn, S.; Kim, G.; Lee, J.-U.; Ma, K. Y.; Jang, A.-R.; Lim, H.; Kim, D.; Ryu, S., Probing evolution of twist-angle-dependent interlayer excitons in $MoSe_2$/WSe_2 van der Waals heterostructures. *ACS Nano* **2017,** *11* (4), 4041-4050.
7. Cho, C.; Wong, J.; Taqieddin, A.; Biswas, S.; Aluru, N. R.; Nam, S.; Atwater, H. A., Highly Strain-Tunable Interlayer Excitons in MoS_2/WSe_2 Heterobilayers. *Nano Lett.* **2021,** *21* (9), 3956-3964.
8. Ye, T.; Li, J.; Li, D., Charge-Accumulation Effect in Transition Metal Dichalcogenide Heterobilayers. *Small* **2019,** *15* (42).
9. Hanbicki, A. T.; Chuang, H.-J.; Rosenberger, M. R.; Hellberg, C. S.; Sivaram, S. V.; McCreary, K. M.; Mazin, I. I.; Jonker, B. T., Double Indirect Interlayer Exciton in a $MoSe_2$/WSe_2 van der Waals Heterostructure. *ACS Nano* **2018,** *12* (5), 4719-4726.
10. Wang, T.; Miao, S.; Li, Z.; Meng, Y.; Lu, Z.; Lian, Z.; Blei, M.; Taniguchi, T.; Watanabe, K.; Tongay, S.; Smirnov, D.; Shi, S.-F., Giant Valley-Zeeman Splitting from Spin-Singlet and Spin-Triplet Interlayer Excitons in WSe_2/$MoSe_2$ Heterostructure. *Nano Lett.* **2020,** *20* (1), 694-700.
11. Ciarrocchi, A.; Unuchek, D.; Avsar, A.; Watanabe, K.; Taniguchi, T.;is, A., Polarization switching and electrical control of interlayer excitons in two-dimensional van der Waals heterostructures. *Nat. Photonics* **2019,** *13* (2), 131-+.
12. Kim, J.; Jin, C.; Chen, B.; Cai, H.; Zhao, T.; Lee, P.; Kahn, S.; Watanabe, K.; Taniguchi, T.; Tongay, S.; Crommie, M. F.; Wang, F., Observation of ultralong valley

lifetime in WSe_2/MoS_2 heterostructures. *SCIENCE ADVANCES* **2017,** *3* (7).
13. Xia, J.; Yan, J.; Wang, Z.; He, Y.; Gong, Y.; Chen, W.; Sum, T. C.; Liu, Z.; Ajayan, P. M.; Shen, Z., Strong coupling and pressure engineering in WSe_2–$MoSe_2$ heterobilayers. *Nat. Phys.* **2021,** *17* (1), 92-98.

Table S1. The parameters of WSe_2/WS_2 heterostructure with different twist angles after relaxation. d is the interlayer distance. E_b is the binding energy and E_{total} is the total energy of the system.

	d (Å)	E_b (eV/cell)	E_{total} (eV/cell)
0°	6.20878	0.29962	-47.43472
27.8°	6.49819	0.24019	-47.37554
38.2°	6.49278	0.24033	-47.37549
60°	6.24729	0.29821	-47.43346

Table S2. The summarized research on interlayer exciton

Structure	Method	Interlayer exciton type	Reference
stacked MoS_2/WSe_2	strain+PL	indirect interlayer exciton	[7]
stacked WS_2/WSe_2	power dependent PL	direct interlayer exciton	[8]
stacked $MoSe_2/WSe_2$	circularly polarized PL	indirect interlayer exciton	[9]
stacked $WSe_2/MoSe_2$	circularly polarized PL+magnetic field dependent PL+gate voltage dependent PL	direct interlayer exciton	[10, 11]
stacked WSe_2/MoS_2	ultrafast pump-probe spectroscopy	direct interlayer exciton	[12]
CVD growth $WSe_2/MoSe_2$	diamond anvil cell+PL+DFT	direct and indirect interlayer exciton	[13]
stacked WSe_2/WS_2	twist angle+circularly polarized PL+ gate voltage-dependent PL+DFT	direct and indirect interlayer exciton	**This work**

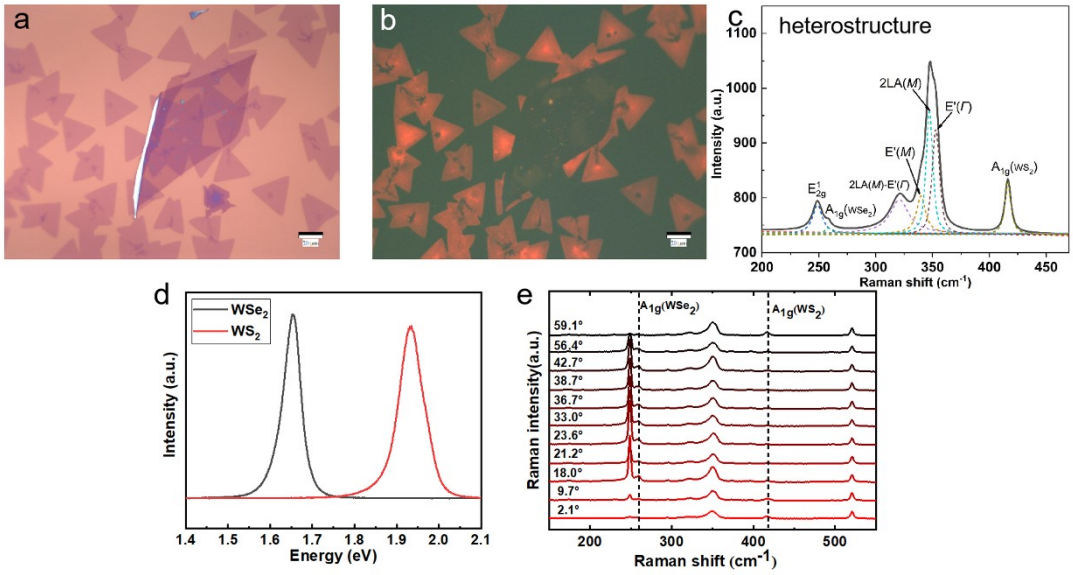

Fig. S1 (a) Optical image of the WSe_2/WS_2 heterostructure with different twist angles. (b) The corresponding FL image of the WSe_2/WS_2 heterostructures with different twist angles shown in (a). (c) The Raman spectrum of the WSe_2/WS_2 heterostructure. (d) The typical PL spectra of monolayer WSe_2 and WS_2. (e) The Raman spectra of WSe_2/WS_2 heterostructure with different twist angles.

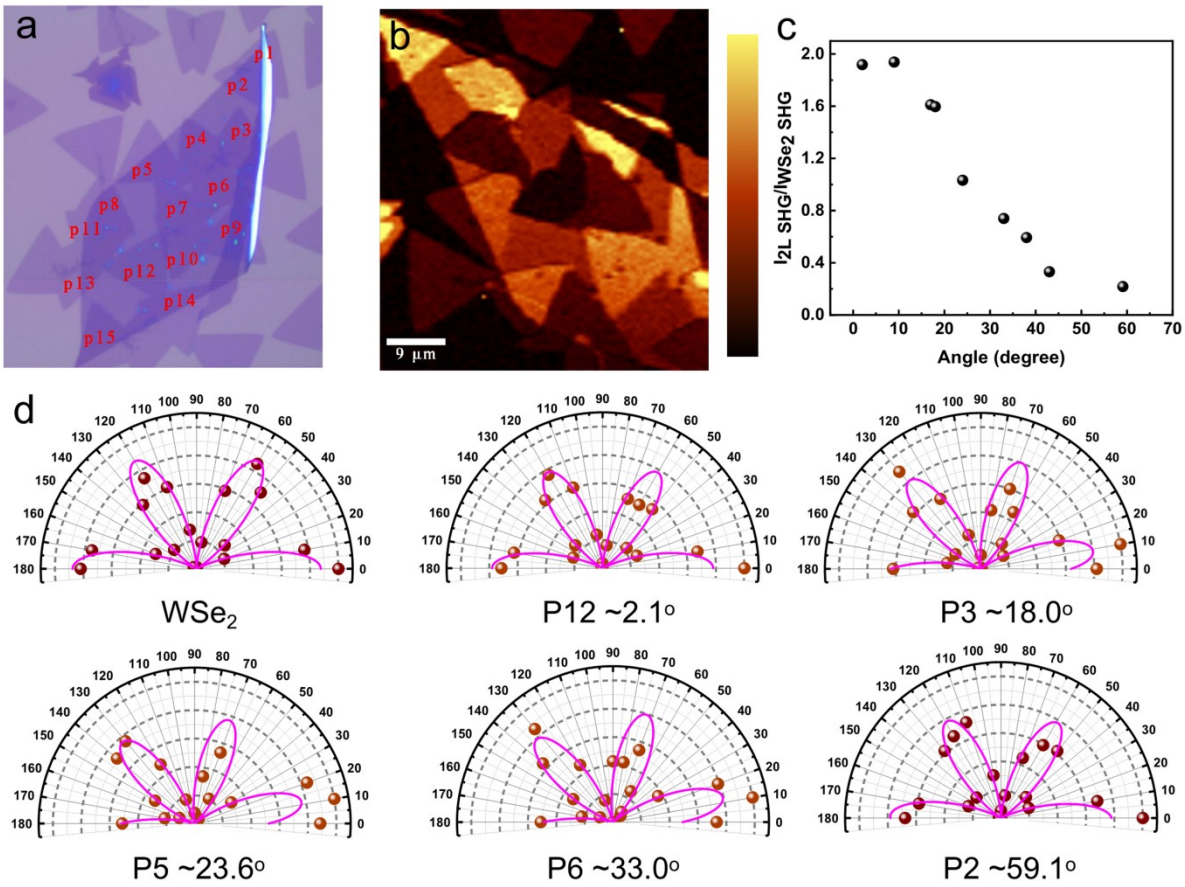

Fig. S2 (a) Optical image of the WSe_2/WS_2 heterostructure with different twist angles. (b) The SHG intensity mapping of the WSe_2/WS_2 heterostructure with different twist angles. (c) The ratio of SHG signal ($I_{Heterostructure}/I_{WS_2}$) as a function of twist angle. (d) Typical SHG measurements of WSe_2/WS_2 heterostructure with different twist angles.

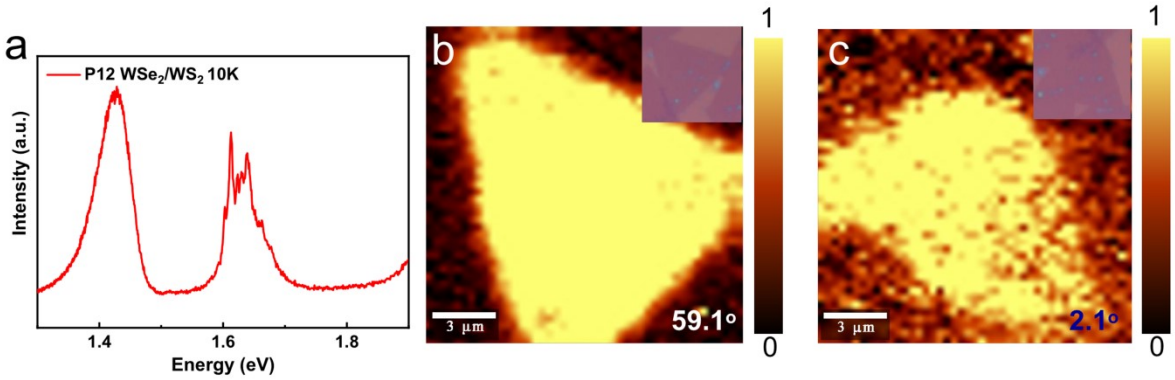

Fig. S3 (a) The PL spectrum of WSe_2/WS_2 heterostructure for sample p12. (b) and (c) are the intensity mapping of interlayer exciton of WSe_2/WS_2 heterostructure with a twist angle of 59.1° and 2.1°, respectively.

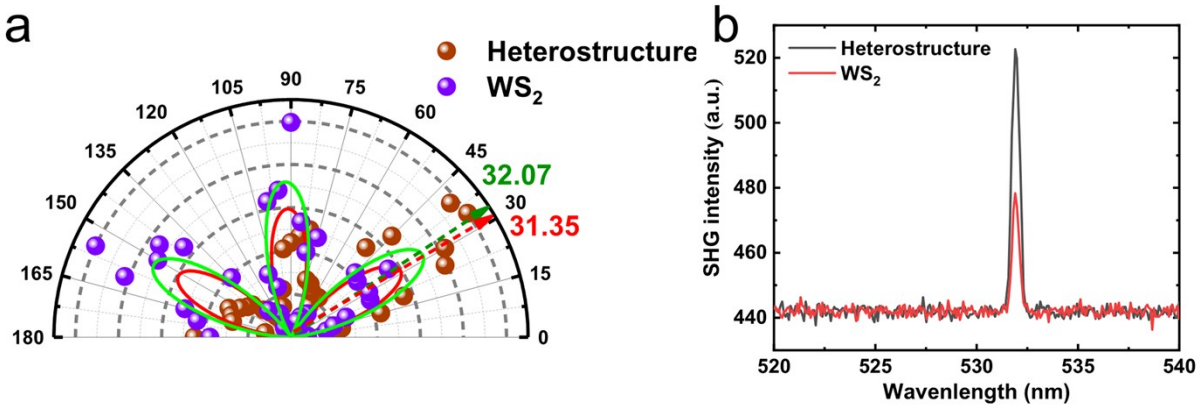

Fig. S4 (a) and (b) are the SHG measurements of the WSe_2/WS_2 heterostructure fabricated by the CVD-grown sample.

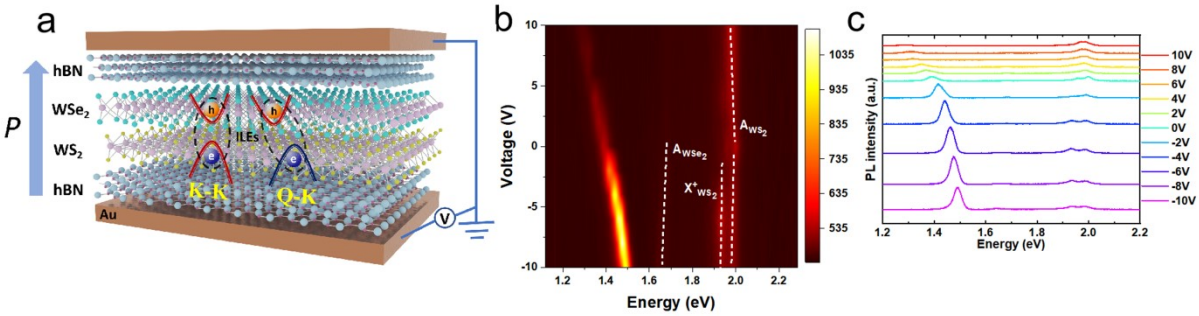

Fig. S5 (a) The schematic of the gate voltage-dependent PL measurement. (b) Color plot of the PL intensity as a function of the gate voltage. (c) PL spectra at the gate voltage of ±10, ±8, ±6, ±4, ±2, and 0 V.

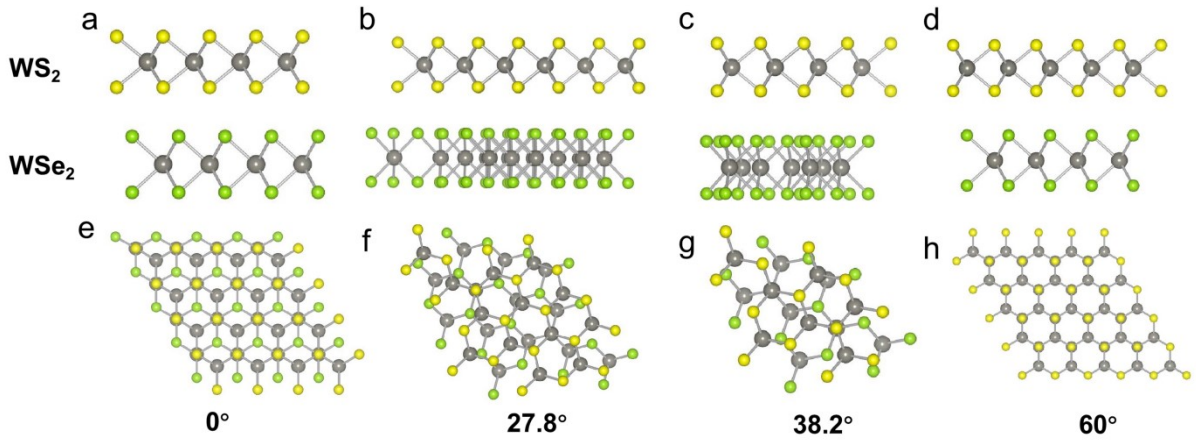

Fig. S6 (a)-(d) are the side-view of WSe_2/WS_2 heterostructure with twist angle of 0^o, 27.8^o, 38.2^o and 60^o, respectively. (e)-(h) are the top-view of WSe_2/WS_2 heterostructure with twist angle of 0^o, 27.8^o, 38.2^o and 60^o, respectively.

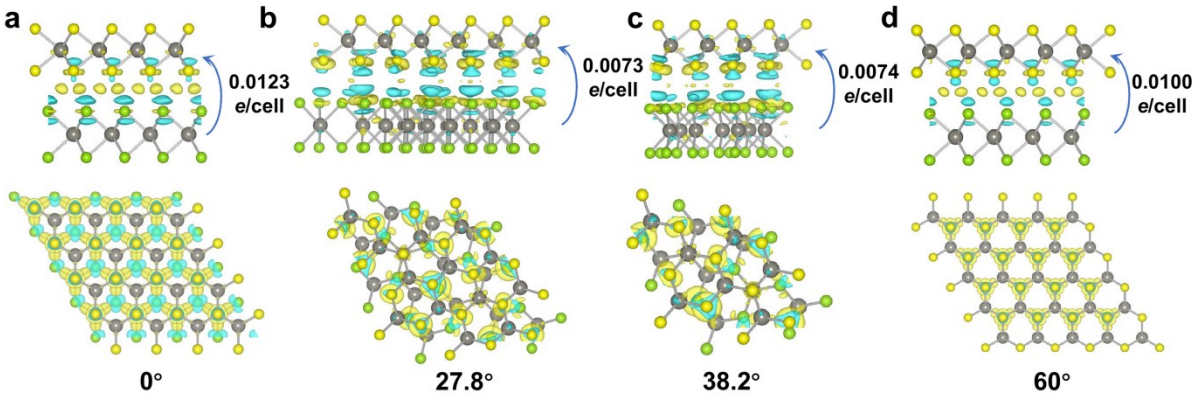

Fig. S7 (a)-(d) are the differential charge densities of WSe_2/WS_2 heterostructures with different twist angles, the isosurface level=2E-4.

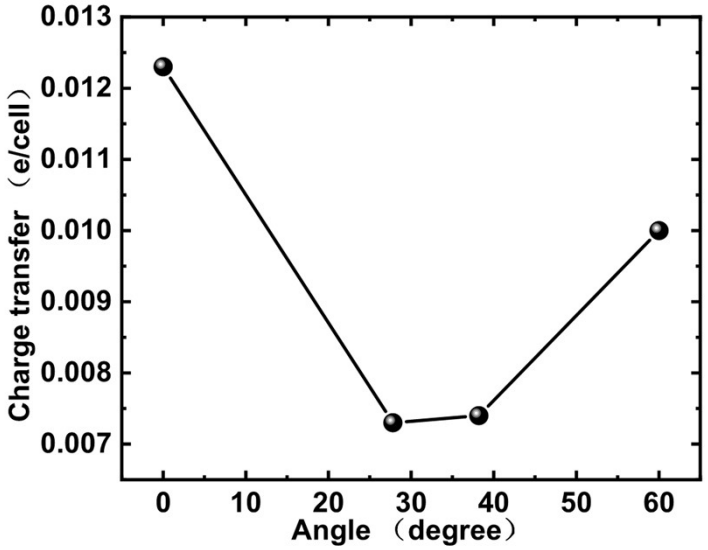

Fig. S8 The charge transfer versus the twist angles of WSe_2/WS_2 heterostructure.